AIAA-98-3704
Influences of Combustion Dynamics on Linear and Nonlinear Unsteady Motions in Solid Propellant Rockets

Fred E.C. Culick, Giorgio Isella, and Claude Seywert
California Institute of Technology
Pasadena, California

34th AIAA/ASME/SAE/ASEE
Joint Propulsion Conference & Exhibit
July 13-15, 1998 / Cleveland, OH

INFLUENCES OF COMBUSTION DYNAMICS ON LINEAR AND NONLINEAR UNSTEADY MOTIONS IN SOLID PROPELLANT ROCKETS

F.E.C. CULICK*, G. ISELLA**, AND C. SEYWERT**

ABSTRACT. This paper is a report of work in progress, part of the Caltech MURI Program: Novel Energetic Materials to Stabilize Rocket Motors. The primary technical objective of the MURI Program is to understand the connections between propellant composition and chemistry, and the dynamical behavior observed in solid propellant rocket motors. Here we are concerned with the theoretical framework in which chamber dynamics are investigated; and certain aspects of combustion dynamics represented by the response function which is ultimately the macroscopic realization of the propellant chemistry and combustion. Some results are given to illustrate possible influences of the frequency spectrum of the response function on linear and nonlinear motions in a solid rocket. A simple model is described which is extended eventually to provide a way to model phenomenologically some of the observed characteristics of the combustion dynamics of a burning solid propellant.

1. INTRODUCTION

Understanding combustion instabilities requires a theoretical framework within which one may interpret experimental results, design laboratory and full-scale tests, and predict the behavior to be expected. This paper is concerned largely with some aspects and applications of spatial averaging as a basis for approximate analysis. This approach serves as an important part of the Caltech MURI program, *Novel Energetic Materials to Stabilize Rocket Motors*[1], in our effort to establish relations between propellant chemistry and the dynamical behavior observed in motors.

The basic technical objective of the Caltech MURI is to understand how small changes in the propellant composition affect the stability of motions in a solid propellant combustor. Figure 1 shows the general technical scheme of the program, indicating external communications as well as interactions between the people engaged in the three tasks. Task 1 is devoted to fundamental chemistry and chemical kinetics, including experimental and theoretical work directed to determining, *inter alia*, rate constants and kinetic mechanisms. Work is being done principally on energetic ingredients, both oxidizers and binders. The results of Task 1 relate to and influence Task 2 in respects not covered in this paper.

Work in Task 2 includes laboratory tests for unsteady and steady burning of energetic ingredients and propellants, including aluminum. It is a central aim of these efforts to acquire data and to understand the influences of new ingredients, and possible effects of small changes in composition on both the steady burning characteristics and the dynamical response of a burning propellant to fluctuations of external variables, chiefly pressure and radiation. Based on the experimental results and previous analyses, models of steady and unsteady burning are being constructed. As part of the overall objective of the MURI program, it is a major purpose of the modeling to account for the effects of compositional changes, small or large, on combustion dynamics and ultimately on the dynamics observed in a motor.

---

*Richard L. and Dorothy M. Hayman Professor of Mechanical Engineering and Professor of Jet Propulsion, California Institute of Technology.

**Graduate Research Assistant.

[1]URL address: http://www.cco.caltech.edu/~culick/muri.html

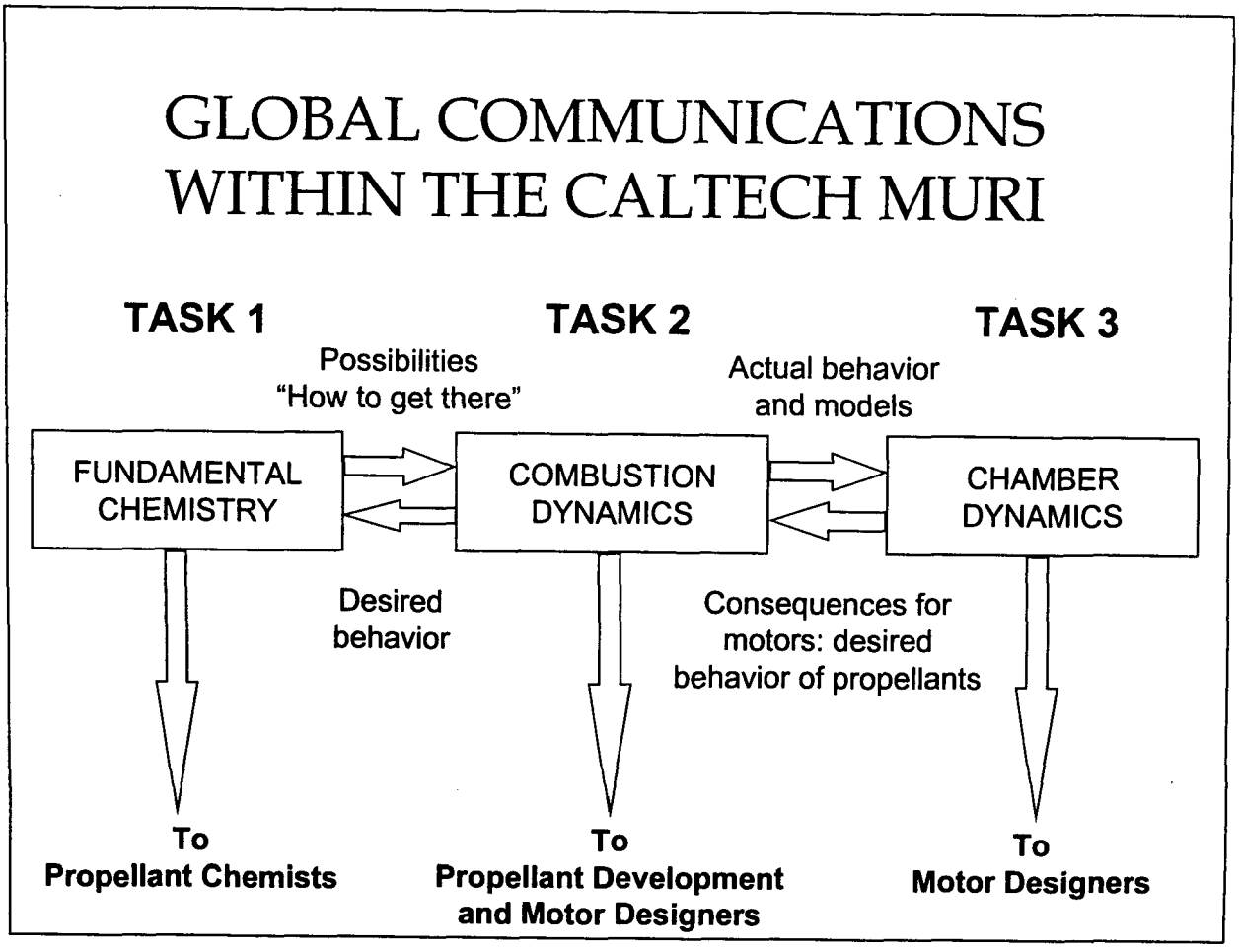

FIGURE 1.1. Interactions between groups in the Caltech MURI program.

The primary connection between Tasks 2 and 3 is the combustion dynamics conventionally, and conveniently, represented by a response function. Strictly, in the context of its traditional definition, a response function is a concept arising with linear behavior, defined here as the dimensionless ratio of a small change of mass flux of gas from a burning surface to a small change of imposed pressure or velocity parallel to the surface. In practice, admittance, impedance, or response functions are almost always introduced for steady oscillations and are therefore complex functions of frequency, i.e., possessing both amplitude and phase. It is possible to introduce, simply as a definition, an analogous function for nonlinear behavior, dependent on amplitude and therefore defined in the time domain. However, this notion has received little attention and nonlinear relations between fluctuations of the burning rate and flow variables are known mainly as implied functions to be extracted from experimental data or from numerical simulations.

Thus in principle, we can understand connections between chamber dynamics and chemical dynamics by constructing suitably detailed models of the combustion dynamics and incorporating the results in the analyses of Task 3. The modeling activities of Task 2 therefore are central to the primary goal of the MURI program but cannot be accomplished without the fundamental results promised in Task 1 and the combustion tests of Task 2.

Despite its central position in the theory, the response function, or more generally combustion dynamics, is not the sole contribution to stability and dynamics of a chamber. What finally appears as the dynamical behavior of a chamber are the consequences of a coupled system comprising the

combustion dynamics; the dynamics of the medium in which the combustion processes take place; and the interactions between the two subsystems. The emphasis in this paper is largely on an analytical framework for treating the coupled system and on several phenomena that arise from the nonlinear fluid mechanics of the medium.

Hence the next section of the paper is concerned with the construction of the equations used in the approximate analysis. In addition to the choice of the partial differential equations (a matter of expansion and ordering in small parameters), there are three essential defining features of the kind of analysis used here: choice of independent variable (we use the time-dependent pressure); choice of spatial basis functions to be used in synthesis of the general pressure field (we use the unperturbed classical acoustic modes appropriate to the geometry and boundary conditions in question); and spatial averaging with respect to a weighting function, here, as usually, chosen to be one of the basis functions. The procedure followed — spatial averaging with a modal expansion of the unsteady pressure field — has been described elsewhere in many places (e.g., references [1] – [4]). It is briefly reiterated here because we wish to compare and explain differences and similarities with an extended form of Galerkin's method used extensively many years ago by Zinn and his students (references [5] – [8]).

In our work we have applied the method based on modal expansion, which leads to a system of coupled nonlinear ordinary second-order differential equations. Each of the equations is associated with an acoustic mode, one term of the expansion, and governs the time evolution of the amplitude of that mode. Thus the equations represent the behavior of a set of coupled nonlinear oscillators. Their solution gives the time evolution of the pressure accompanying unsteady motions in a combustor. Because the solutions are oscillatory, numerical simulations are often time consuming and expensive. The procedure is greatly eased by applying time averaging to give a system of first-order equations governing the slowly varying magnitude and phase of the modal amplitudes.

In Section 3 of this paper, we give some results obtained with this method applied to instabilities in a cylindrical rocket motor. The purpose is to show some influences of the shape of the response function for combustion dynamics on properties of limit cycles. These results are intended to illustrate the point made above: (1) fundamental combustion processes determine the characteristics of the combustion dynamics of a burning propellant; (2) the combustion dynamics strongly affect the dynamics of unsteady motions in a chamber; and therefore (3) it is reasonable to seek the connections between details of propellant composition on the one hand, and the linear and nonlinear behavior of unsteady motions in a solid rocket motor.

The last section of the paper covers a model of the dynamics for a burning propellant, formulated to accommodate transient behavior in the condensed phase, the gas phase, and in a thin region adjacent to the interface of the condensed phase. The analysis amounts to an extension of the familiar 'QSHOD' theory, partly to provide a simple framework in which detailed modeling of surface dynamics can be treated. A primary motivation is to gain some understanding of observed departures of data for response functions from the predictions of the QSHOD model which accounts only for the dynamics of the thermal waves in the condensed phase. Although the model treated here is largely phenomenological, it offers possibilities for assessing the relative importance of elementary dynamical processes. At this time, the formalism has been worked out but no quantitative results have been obtained.

2. Comparison of Spatial Averaging Methods Used in Analysis of Combustion Instabilities

The approximate analysis used to investigate combustion instabilities is based on writing all independent variables as sums of averaged and small-amplitude fluctuating parts (e.g., $p = \bar{p} + p'$)). Substitution into the conservation and state equations yields the governing equations for the

fluctuating quantities. Spatial averaging is applied to those equations followed by a modal expansion of the unsteady pressure and velocity fields in order to get a reduced order model of the system. In the literature two different methods for the spatial averaging have been extensively used, one by the first author and his students and one by Zinn and his students. This section compares the two methods.

2.1. **Averaging and Green's Theorem Applied to the Nonlinear Wave Equation.** We combine the conservation equations to form a nonlinear wave equation (2.1) for the unsteady pressure field p'. In this approach the boundary condition for p' is given by equation (2.2). The procedure used to arrive at these equations has been described elsewhere (references [1] – [4]) in full detail:

$$\begin{aligned}\nabla^2 p' - \frac{1}{\bar{a}^2}\frac{\partial^2 p'}{\partial t^2} &= h \\ &= -\bar{\rho}\nabla\cdot(\bar{\mathbf{u}}\cdot\nabla\mathbf{u}' + \mathbf{u}'\cdot\nabla\bar{\mathbf{u}}) + \frac{1}{\bar{a}^2}\bar{\mathbf{u}}\cdot\nabla\frac{\partial p'}{\partial t} + \frac{\gamma}{\bar{a}^2}\frac{\partial p'}{\partial t}\nabla\cdot\bar{\mathbf{u}} \\ &\quad - \bar{\rho}\nabla\cdot\left(\mathbf{u}'\cdot\nabla\mathbf{u}' + \frac{p'}{\gamma\bar{p}}\frac{\partial\mathbf{u}'}{\partial t}\right) + \frac{1}{\bar{a}^2}\frac{\partial}{\partial t}(\mathbf{u}'\cdot\nabla p') \\ &\quad + \frac{\gamma}{\bar{a}^2}\frac{\partial}{\partial t}(p'\nabla\cdot\mathbf{u}') + \nabla\cdot\mathcal{F}' - \frac{1}{\bar{a}^2}\frac{\partial\mathcal{P}'}{\partial t}\end{aligned} \tag{2.1}$$

$$\begin{aligned}-\hat{\mathbf{n}}\cdot\nabla p' &= f \\ &= \bar{\rho}\frac{\partial\mathbf{u}'}{\partial t}\cdot\hat{\mathbf{n}} + \bar{\rho}\,(\bar{\mathbf{u}}\cdot\nabla\mathbf{u}' + \mathbf{u}'\cdot\nabla\bar{\mathbf{u}})\cdot\hat{\mathbf{n}} \\ &\quad + \bar{\rho}(\mathbf{u}'\cdot\nabla\mathbf{u}')\cdot\hat{\mathbf{n}} + \frac{p'}{\bar{a}^2}\frac{\partial\mathbf{u}'}{\partial t}\cdot\hat{\mathbf{n}} - \mathcal{F}'\cdot\hat{\mathbf{n}}\end{aligned} \tag{2.2}$$

In the above equations $\mathcal{F}'$ and $\mathcal{P}'$ describe source terms which arise from the unsteady combustion process and need to be modeled.

The weighting functions for the spatial averaging are chosen to be the unperturbed wave modes ψ_n predicted by classical acoustics for the same combustion chamber with rigid boundaries and no combustion or mean flow. They are obtained by setting $h = f = 0$ in the preceding equations.

$$\nabla^2\psi_n + k_n^2\psi_n = 0 \tag{2.3}$$

$$\hat{\mathbf{n}}\cdot\nabla\psi_n = 0 \tag{2.4}$$

The actual averaging is done by multiplying equation (2.1) by ψ_n, multiplying equation (2.3) by p', subtracting the results and integrating over the volume of the combustion chamber. Applying Greene's theorem and substituting for the boundary conditions the final expression is found:

$$\frac{1}{\bar{a}^2}\int\psi_n\frac{\partial^2 p'}{\partial t^2}dV + k_n^2\int\psi_n p'dV = -\int\psi_n h dV - \oint\psi_n f dS \tag{2.5}$$

For the approximate analysis p' and $\mathbf{u}'$ are expanded using those acoustic modes as a basis:

$$\begin{aligned}p'(\mathbf{x},t) &= \sum_{n=1}^{N}\eta_n(t)\psi_n(\mathbf{x}) && (a) \\ \mathbf{u}' &= \sum_{n=1}^{N}\frac{\dot{\eta}_n(t)}{\gamma k_n^2}\nabla\psi_n(\mathbf{x}) && (b)\end{aligned} \tag{2.6}$$

Substitution in (2.5) leads eventually to the set of coupled oscillator equations

$$\ddot{\eta}_n + \omega_n^2\eta_n = F_n \tag{2.7}$$

where

$$F_n = -\frac{\bar{a}^2}{E_n^2}\left\{\int h\psi_n dV + \oint f\psi_n dS\right\} \tag{2.8}$$

Taking advantage of the presence of two small parameters appearing on the right-hand side (the Mach numbers of the averaged and fluctuating flow fields) one may devise an iteration/perturbation procedure to construct approximate sets of equations. The use of (2.7) and (2.8) constitutes the first step in that process.

2.2. **Modified Galerkin Method.** Zinn *et al.* first developed an alternative approach to spatial averaging which they called 'modified Galerkin method'. Here only a short outline is given; a comprehensive description an be found in references [5] and [6].

In the most general mathematical setting it is assumed that the solution $\mathbf{x}$ to a system of equations fulfills the equations (2.9) in the interior of a volume V and behaves according to equations (2.10) on the boundary of that volume. The E_i are arbitrary mathematical expressions; in the context of combustion instabilities they will be the equations of continuity, momentum and energy, as well as the equation of state. The boundary conditions B_i in the rocket engine application describe the nozzle exit, injector entrance, or surface combustion dynamics:

$$E_i(\mathbf{x}, t) = 0 \qquad i = 1, \ldots, K \tag{2.9}$$

$$B_i(\mathbf{x}, t) = 0 \qquad i = 1, \ldots, K \tag{2.10}$$

In the original Galerkin method an approximate solution $\tilde{\mathbf{x}} = \sum_1^N a_n \varphi_n$ to the above system is constructed in such a way that it fulfills the boundary conditions automatically (i.e., it is assumed that each expansion function φ_n satisfies the equations (2.10)). The 'best' $\tilde{\mathbf{x}}$ is then obtained by spatially averaging the remaining equations over the volume V with some weighting functions ϕ_n (usually taken to be the same as φ_n), thus solving the system (2.11) for the unknowns a_n:

$$\int E_i(\tilde{\mathbf{x}}, t)\,\phi_n dV = 0 \qquad i = 1, \ldots, K \tag{2.11}$$

According to Zinn *et al.*, the condition that the expansion functions fulfill the stringent boundary conditions can be relaxed if those boundary conditions are accounted for in the weighting process itself; this should be done by solving the system (2.12) instead of (2.11). A justification for this approach is given in [7].

$$\int_0^T \left[\int E_i(\tilde{\mathbf{x}}, t)\,\phi_n dV - \oint B_i(\tilde{\mathbf{x}}, t)\,\phi_n dS\right] dt = 0 \tag{2.12}$$

As mentioned, this method can be applied directly to the conservation equations [8]. A simplification (introduced in [5]) is achieved by first forming a wave equation for the velocity potential Φ. In the analysis each perturbation quantity and the mean flow Mach number are taken to be of $O(\epsilon)$, where ϵ is a small ordering parameter that is a measure of the wave amplitude. Neglecting all terms of $O(\epsilon^3)$ and higher, it can be shown that the flow field is irrotational and the conservation equations can be combined with the equation of state to yield equation (2.13). The combustion process is accounted for in the source term W'_m; Zinn *et al.* use Crocco's pressure sensitive time-lag hypothesis to describe the unsteady combustion process, giving eventually

$$\nabla^2\Phi - \frac{\partial^2\Phi}{\partial t^2} = 2\bar{\mathbf{u}}\cdot\nabla\frac{\partial\Phi}{\partial t} + \gamma(\nabla\cdot\bar{\mathbf{u}})\frac{\partial\Phi}{\partial t} + 2\nabla\Phi\cdot\nabla\frac{\partial\Phi}{\partial t} + (\gamma-1)\frac{\partial\Phi}{\partial t}\nabla^2\Phi + W'_m \tag{2.13}$$

The potential Φ is then expanded in a modal series (see equation 2.14) and the modified Galerkin method is applied using the functions ϕ as weighting functions:

$$\Phi(\mathbf{x},t) = \sum_{n=1}^{N} A_n(t)\phi_n(\mathbf{x}) \tag{2.14}$$

Combining the appropriate boundary condition with equation(2.13) and using each of the functions ϕ_n to average the resulting expression leads to set of N differential equations for the A_n. The ϕ_n are chosen such as to coincide with the acoustic modes of the combustion chamber. From Φ the unsteady pressure and velocity fields are recovered using the relations:

$$\mathbf{u}' = \nabla\Phi \tag{2.15}$$

$$p'(\mathbf{x},t) = \gamma\left[\frac{1}{2}\frac{\partial\Phi}{\partial t}^2 - \frac{\partial\Phi}{\partial t} - \bar{\mathbf{u}}\cdot\nabla\Phi - \frac{1}{2}\nabla\Phi\cdot\nabla\Phi\right] \tag{2.16}$$

2.2.1. *Comparison.* Since the 'modified Galerkin method' is quite general it can be applied directly to the equations given by Culick, i.e., equation (2.1) with boundary condition (2.2). According to equation (2.12) the result is given by (2.17):

$$\int\left(\nabla^2 p' - \frac{1}{\bar{a}^2}\frac{\partial^2 p'}{\partial t^2} - h\right)\phi_n dV - \oint\left(\hat{\mathbf{n}}\cdot\nabla p' + f\right)\phi_n dS = 0 \tag{2.17}$$

This equation can be rewritten to give:

$$\frac{1}{\bar{a}^2}\int\frac{\partial^2 p'}{\partial t^2}\phi_n dV - \int\nabla^2 p'\phi_n dV + \oint\hat{\mathbf{n}}\cdot\nabla p'\phi_n dS = -\int h\phi_n dV - \oint f\phi_n dS \tag{2.18}$$

Making use of Greene's theorem it can be seen that:

$$-\int\nabla^2 p'\phi_n dV = \oint\left(p'\nabla\phi_n - \phi_n\nabla p'\right)\cdot\hat{\mathbf{n}}dS - \int p'\nabla^2\phi_n dV \tag{2.19}$$

If the weighting functions ϕ_n are now chosen to coincide with the functions ψ_n as defined and used above (equations 2.3 and 2.4) this last equation turns into

$$-\int\nabla^2 p'\phi_n dV = \oint\left(0 - \psi_n\nabla p'\cdot\hat{\mathbf{n}}\right)dS + k_n^2\int p'\psi_n dV \tag{2.20}$$

Substituting (2.20) in equation (2.18) the integral equation (2.5) for the pressure is recovered:

$$\frac{1}{\bar{a}^2}\int\psi_n\frac{\partial^2 p'}{\partial t^2}dV + k_n^2\int\psi_n p' dV = -\int\psi_n h dV - \oint\psi_n f dS \tag{2.21}$$

Thus the averaging methods used in both approaches yield exactly the same results *when applied to the nonlinear pressure wave equation.* In particular the boundary conditions are handled in the same manner.

Discrepancies in the results reported by both authors arise due to the fact that the averaging is applied to different equations (e.g., equations 2.1 versus 2.13) and because both authors expand different physical quantities ($p' = \sum_1^N \eta_n\psi_n$ or $\Phi = \sum_1^N A_n\phi_n$). Among other things, those differences cause difficulties when one tries to understand similarities and differences between the two approaches. We will treat that matter thoroughly in a subsequent report.

3. Some Effects of the Shape of the Response Function on Chamber Dynamics

The procedure described in the previous section, after substitution of the expansion for the pressure in the nonlinear wave equation and after appropriate spatial averaging (see, e.g., references [1] - [4]), eventually leads to a set of equations for the amplitudes $\eta_n(t)$ that can be written as

$$\frac{d^2\eta_n}{dt^2} + \omega_n^2 \eta_n = F_n \tag{3.1}$$

where the forcing function is

$$F_n = -\frac{1}{E_n^2}\left\{\int h\psi_n dV + \oiint f\psi_n dS\right\} \tag{3.2}$$

and

$$E_n^2 = \int \psi_n^2 dV \tag{3.3}$$

These form a set of coupled oscillators. For second-order acoustics, F_n has the following expression (reference [1]):

$$\ddot{\eta}_n + \omega_n^2 \eta_n = -\sum_i \left[D_{ni}\dot{\eta}_i + E_{ni}\eta_i\right] - \sum_{i=1}^{\infty}\sum_{j=1}^{\infty}\left[A_{nij}\dot{\eta}_i\dot{\eta}_j + B_{nij}\eta_i\eta_j\right] \tag{3.4}$$

The constants D_{ni}, E_{ni}, A_{nij}, B_{nij} depend on the unperturbed mode shapes and frequencies and on the mean flow field.

Numerical computations presented in this paper use a time-averaged version of the equations; time averaging is based on the identification of the presence of two time-scales: a *fast* scale, proportional to the period of the oscillation, and a *slow* scale, which characterizes the relatively gradual variations of amplitude and phase. The validity of time-averaging is an open question: its practical validity in the analysis is supported by experimental evidence of the presence of two time scales; from the numerical point of view, previous results have shown agreement between the amplitudes obtained from time averaged and non time-averaged equations (reference [4]). After time averaging, the equations for the amplitudes are (reference [2]):

$$\begin{aligned}
\frac{dA}{dt} &= \alpha_n A_n + \theta_n B_n + \frac{\beta n}{2}\left[A_i\left(A_{n-i} - A_{i-n} - A_{i+n}\right) - B_i\left(B_i(B_{n-i} + B_{i-n} + B_{i+n})\right]\right. \\
\frac{dB}{dt} &= \alpha_n B_n + \theta_n A_n + \frac{\beta n}{2}\left[A_i\left(B_{n-i} + B_{i-n} - B_{i+n}\right) - B_i\left(B_i(A_{n-i} - A_{i-n} + A_{i+n})\right]\right.
\end{aligned} \tag{3.5}$$

The analysis of the effect of the shape of the response function on the combustion dynamics is based on parametric variations of a function expressed in the classical Denison and Baum form (reference [9]):

$$R_b = \frac{nAB}{\lambda_c + A/\lambda_c - (1+A) + AB} \tag{3.6}$$

where $A = 6.0$, $B = 0.55$, $n = 0.3$, $\gamma = 1.18$, and λ is related to the oscillation frequency. The top half of Figure 3.1 presents a plot of the real and imaginary part of this function. The combustion chamber is represented as a cylinder of length 0.5969 m and radius 0.0253 m. Other geometrical characteristics of the chamber and physical properties of the propellant used for computations can be found in [2] and are not repeated here. The frequency of the fundamental mode (first longitudinal mode) is 900 Hz. The presence of a nozzle is taken into account by the use of an appropriate admittance function; further damping is introduced by the presence of particulate material (see [2] for details). The reference response function is chosen so that the first longitudinal mode is unstable, while all the other modes are stable. This feature is preserved in all the parametric variations considered, except for the last example, where the second mode is unstable, all the others stable.

The top part of Figure 3.1 presents the reference response function; the bottom half shows the time history of amplitudes of the first 12 longitudinal modes. The real part of the response function is in blue, the imaginary part in green. Vertical color-coded lines mark the frequencies of the modes retained in the calculations; the corresponding amplitude is traced in the same color in the bottom picture. The table below the figure reports the growth constant (positive value indicates an unstable mode), the frequency shift and the limit amplitude of the mode in the limit cycle. The growth constants (α_n) and frequency shifts (θ_n) include all the contributions described above: propellant response function, nozzle impedance and particle damping. Note the very negative values of the α_n at high frequency: this is mainly caused by damping due to solid particles; the propellant response has a destabilizing effect at all frequencies, as shown by the picture in the top half of Figure 3.1, the nozzle has a damping effect which can be considered independent of frequency (see [2] for details). As shown by the simulation results, the first mode, unstable, transfers energy to higher frequency modes, until a balance is reached and the system settles into a stable limit cycle, involving all the modes, also the ones with very high damping. This is a typical result, normally obtained through simulations based on the described method ([1] –[4]).

The second picture (Figure 3.2) shows the result of the same calculation, with all θ_n set to zero. As it clear from the figure and the limit values, the effect of θ on the dynamic of the limit cycle is almost irrelevant for the conditions assumed here.

Figure 3.3 presents the effect of a reduced particle damping (the damping is only reduced and not eliminated, since a complete elimination of particle damping would lead to a growth of the amplitudes well further the limits set by the present approximations). The results show a maximum amplitude of the first mode higher than before, as expected. A surprising result is the different dynamic behavior of higher modes: the final amplitude of the 12th mode is the 4th in magnitude and also other high frequency modes (8 and 10) have relatively high values. This fact can play a role in the instabilities of real systems, since the damping effect of particles might not always be so high as in our model, and also it might not be increasing uniformly with frequency as it is supposed here. A physical explanation of this phenomenon is not available at this time.

The effect of a change in shape of the response function is analyzed in Figure 3.4. In this case a second peak at higher frequency has been added to the real part of R_b. The imaginary part is constant in all the examples, since it has been assessed that θ has little or no influence on the dynamics we are considering. Also in this case the effect is surprising: we are adding destabilizing contribution to the system (the R_b is overall *more* positive, as also shown by less negative values of the growth constants); even so, the amplitude of the limit cycle is *decreased* by almost 15% (compare with Figure 3.1). This could be justified by the observation that the modes at higher frequency are now more active (since they are less damped, they play a bigger role in the dynamics of the system), and they can contain more energy at lower amplitude, compared to the first case where most of the energy has to be stored in a low frequency mode. For this case, setting θ_n to zero, or reducing the particulate damping has the same relative effect as the first example presented.

A response function with only one broad peak in the real part is presented in Figure 3.5. This case differs from the previous in that the first mode is stable, the second is unstable. The mode contribution to the limit cycle is quite different: instead of involving all the modes as before, now only the even modes are excited. The amplitude of the limit cycle is also consistently lower than before, in agreement with the observation above.

For this case, reducing the particle damping until close to instability of the system, has a dramatic effect on the dynamics, as shown in Figure 3.6. After a long transient, all the modes results in being excited, and the higher frequency modes are at a larger amplitude than the reference case (Figure 3.5). In this case we observed that θ_n are important in the calculations: if set to zero, all that part of the dynamics is lost, and the result looks quite different (Figure 3.7).

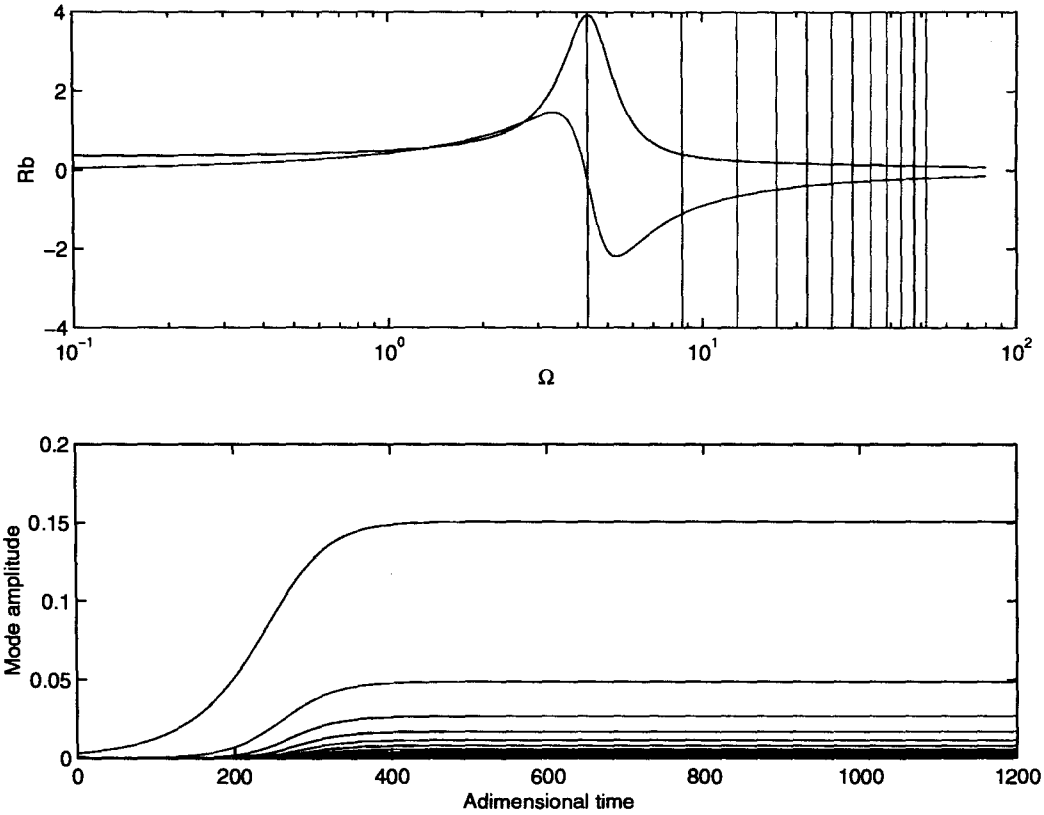

Mode	α_n	ϑ_n	Limit amplitude
1	82.	34.	0.150
2	-316.	101.	0.048
3	-561.	117.	0.026
4	-873.	196.	0.0169
5	-1255.	334.	0.0114
6	-1703.	539.	0.00796
7	-2214.	820.	0.00564
8	-2785.	1186.	0.00404
9	-3412.	1648.	0.00292
10	-4092.	2217.	0.00210
11	-4821.	2903.	0.00157
12	-5595.	3715.	0.00138

FIGURE 3.1. Reference response function, AB form.

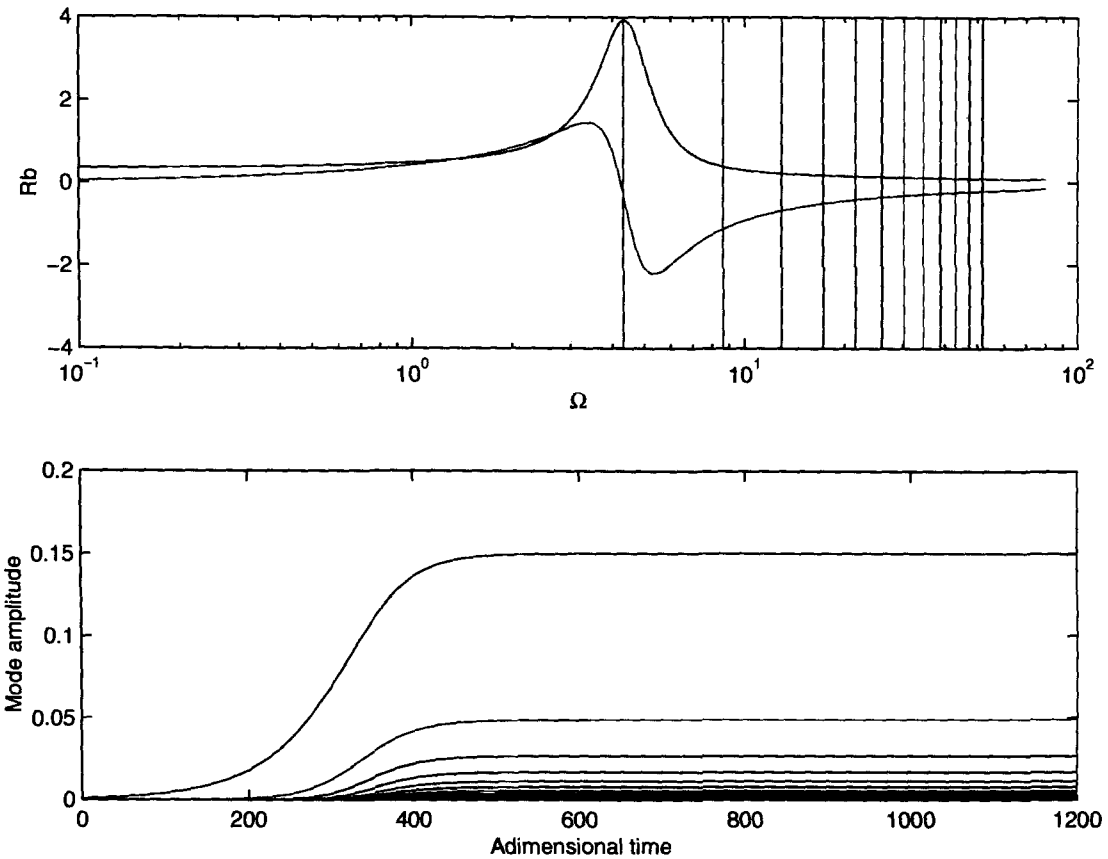

Mode	α_n	ϑ_n	Limit amplitude
1	82.	0.0	0.150
2	-316.	0.0	0.0486
3	-561.	0.0	0.0267
4	-873.	0.0	0.0169
5	-1255.	0.0	0.0114
6	-1703.	0.0	0.00789
7	-2214.	0.0	0.00557
8	-2785.	0.0	0.00399
9	-3412.	0.0	0.00288
10	-4092.	0.0	0.00213
11	-4821.	0.0	0.00152
12	-5595.	0.0	0.00160

FIGURE 3.2. Reference R_b. Simulation with $\theta_n = 0$.

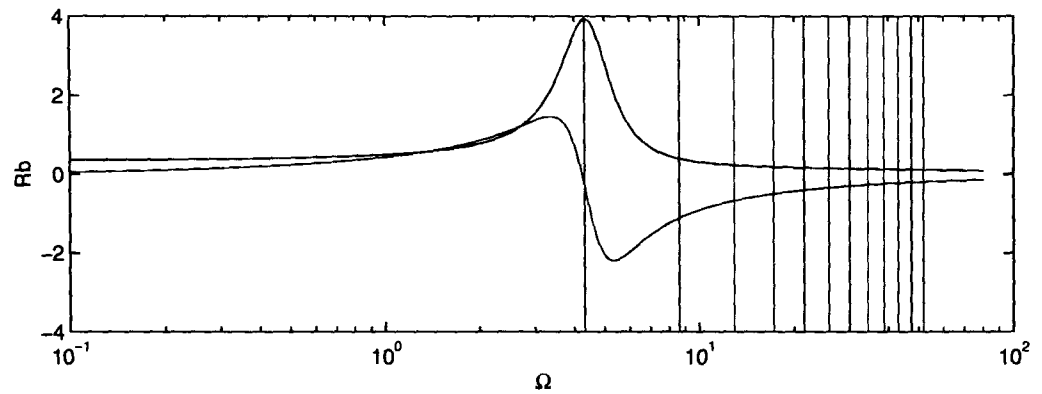

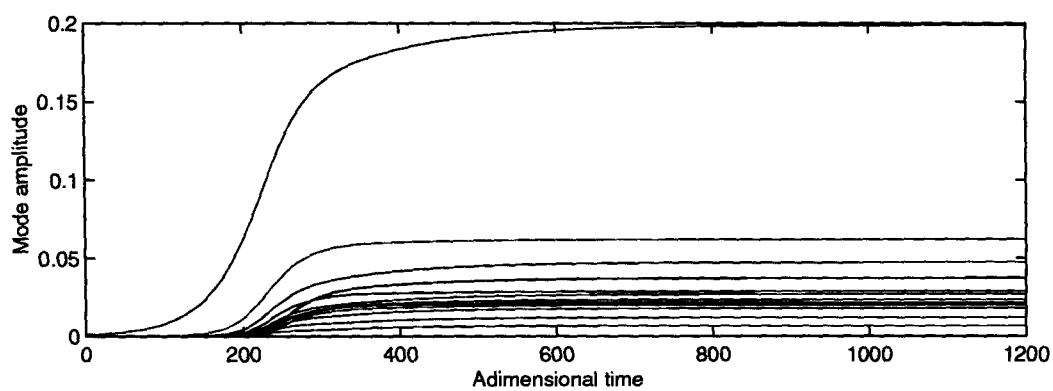

Mode	α_n	ϑ_n	Limit amplitude
1	119.	32.	0.199
2	-168.	84.	0.0619
3	-226.	62.	0.0473
4	-292.	68.	0.0288
5	-369.	90.	0.0269
6	-460.	127.	0.0214
7	-562.	181.	0.0179
8	-677.	253.	0.0201
9	-803.	344.	0.0120
10	-939.	456.	0.0234
11	-1085.	592.	0.00669
12	-1240.	754.	0.0371

FIGURE 3.3. Reduced particle damping (20% of the original).

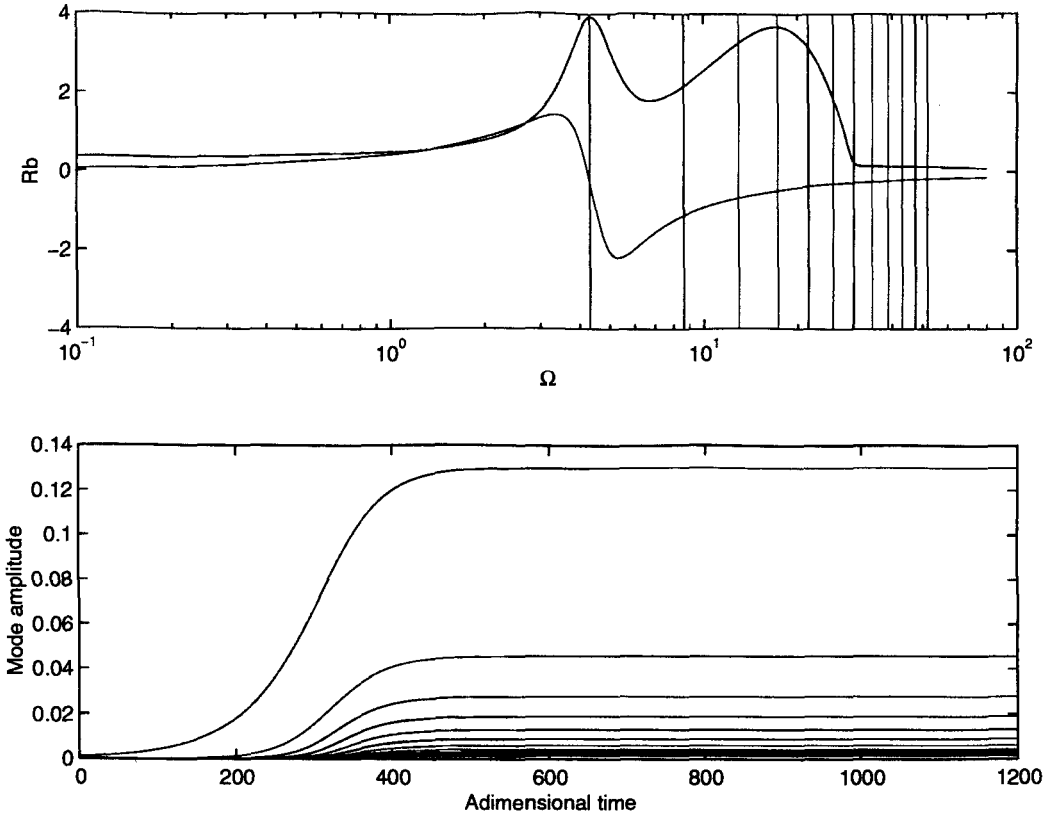

Mode	α_n	ϑ_n	Limit amplitude
1	82.	34.	0.130
2	-184.	101.	0.0457
3	-334.	117.	0.0280
4	-616.	196.	0.0190
5	-1038.	334.	0.0131
6	-1587.	539.	0.00897
7	-2212.	820.	0.00611
8	-2785.	1186.	0.00434
9	-3412.	1648.	0.00314
10	-4092.	2217.	0.00228
11	-4821.	2903.	0.00171
12	-5595.	3715.	0.00146

FIGURE 3.4. Modified response function; a second peak at high frequency has been added.

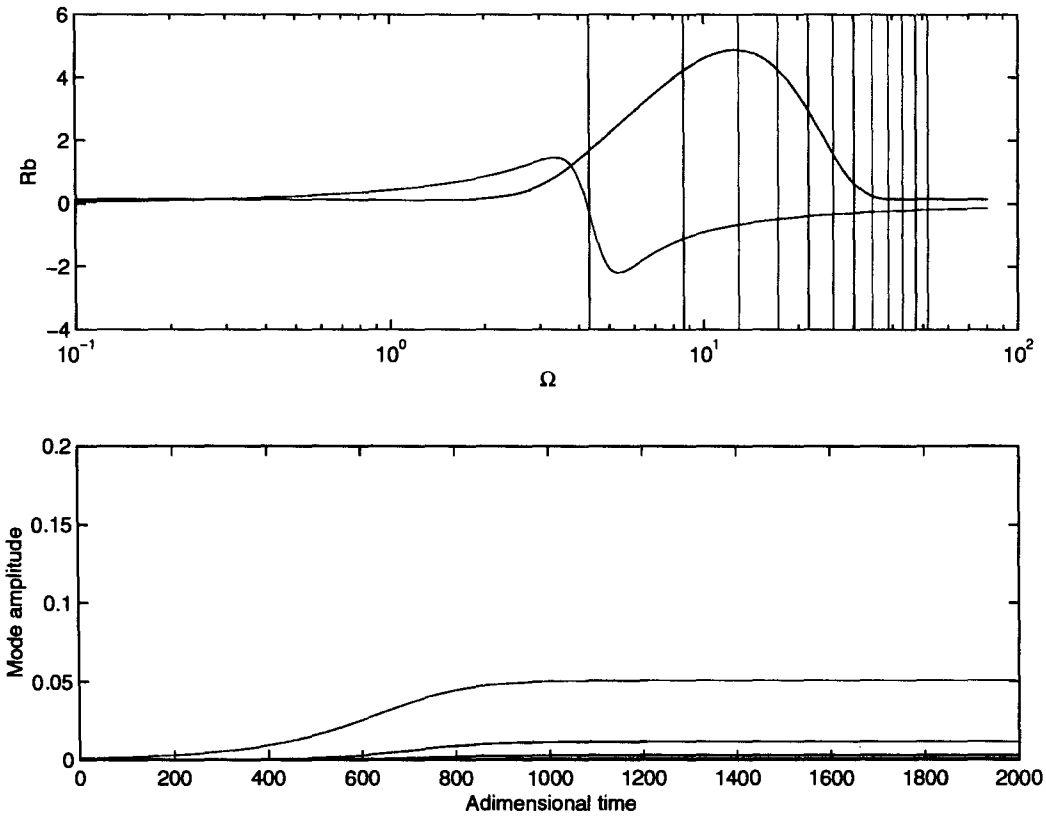

Mode	α_n	ϑ_n	Limit amplitude
1	-16.	34.	0.000023
2	31.	101.	0.0506
3	-155.	117.	0.000026
4	-514.	196.	0.0115
5	-992.	334.	0.000010
6	-1541.	539.	0.00275
7	-2117.	820.	0.000003
8	-2714.	1186.	0.000726
9	-3347.	1648.	0.000001
10	-4026.	2217.	0.000197
11	-4754.	2903.	0.000000
12	-5528.	3715.	0.000054

FIGURE 3.5. *Broad-peak* response function. Note that in this case the second mode is unstable.

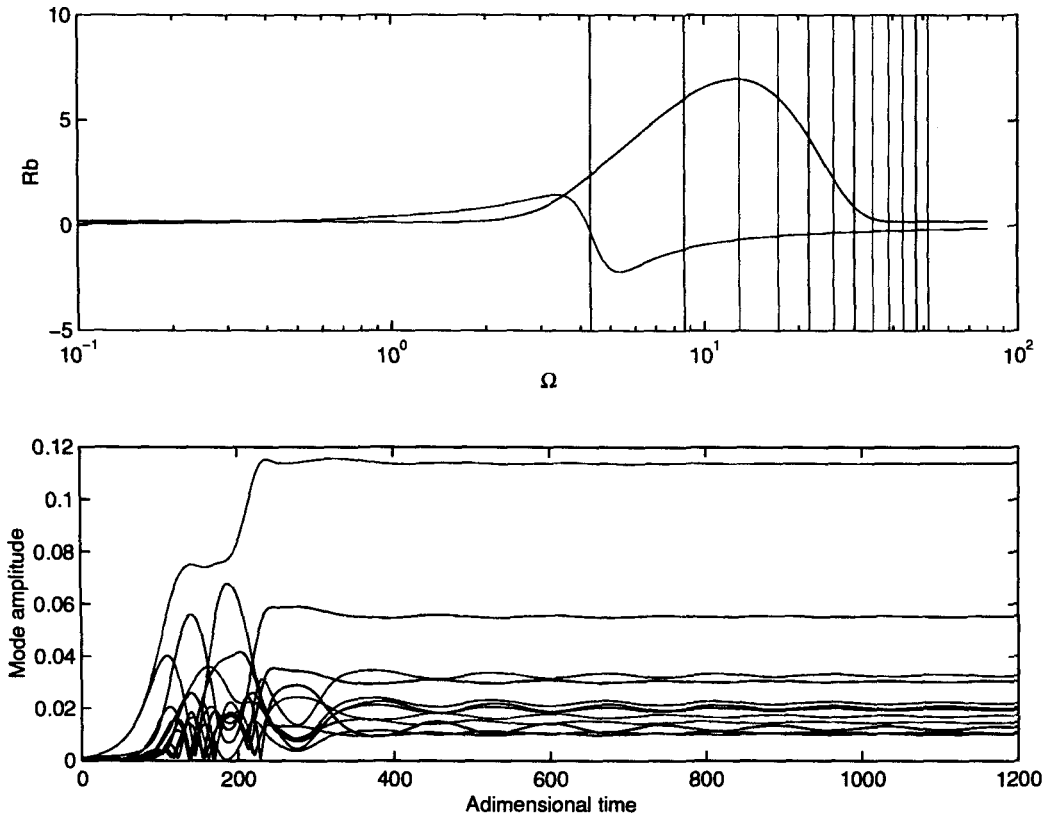

Mode	α_n	ϑ_n	Limit amplitude
1	5.	32.	0.0147
2	230.	86.	0.114
3	226.	69.	0.0201
4	63.	84.	0.0554
5	-191.	121.	0.0220
6	-471.	179.	0.0304
7	-717.	261.	0.0195
8	-928.	369.	0.0173
9	-1124.	507.	0.0107
10	-1327.	676.	0.0102
11	-1546.	881.	0.0326
12	-1778.	1124.	0.0127

FIGURE 3.6. Several unsteady modes complicate the dynamic behavior of the system.

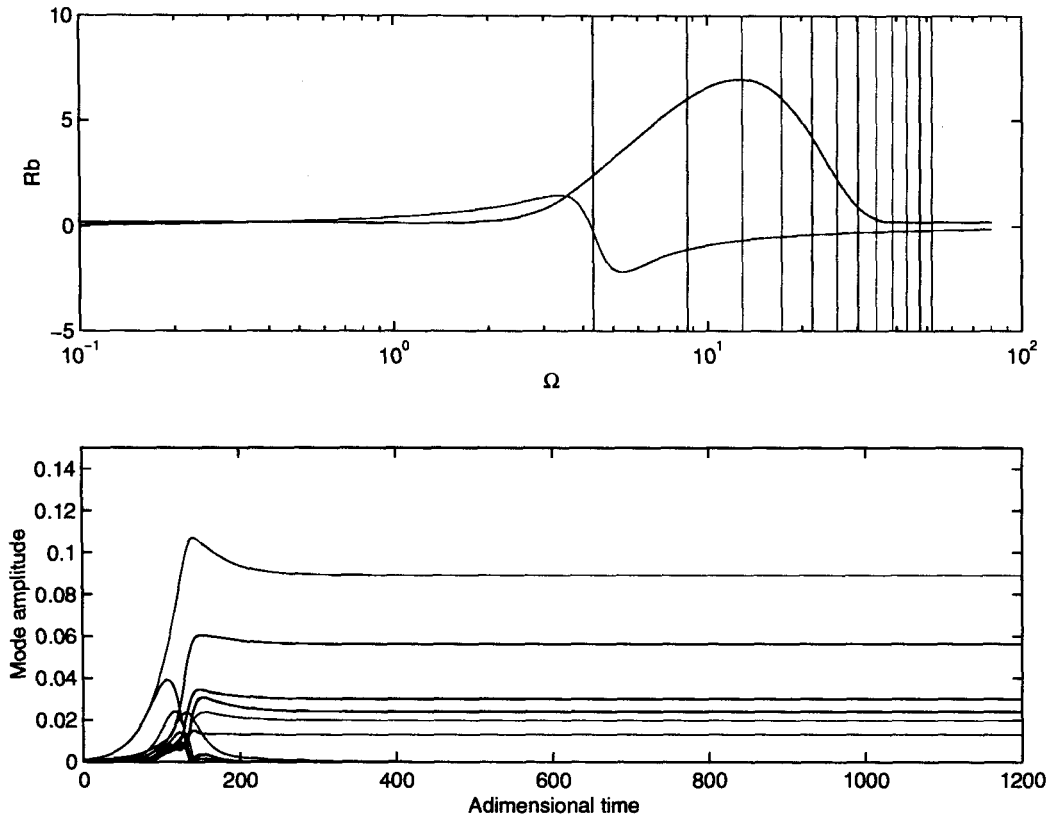

Mode	α_n	ϑ_n	Limit amplitude
1	5.	0.0	0.000023
2	230.	0.0	0.0891
3	226.	0.0	0.000094
4	63.	0.0	0.0562
5	-191.	0.0	0.000079
6	-471.	0.0	0.0300
7	-717.	0.0	0.000063
8	-928.	0.0	0.0197
9	-1124.	0.0	0.000052
10	-1327.	0.0	0.0129
11	-1546.	0.0	0.000121
12	-1778.	0.0	0.0240

FIGURE 3.7. For this case (cf. Figure 3.6) the presence of θ_n is important.

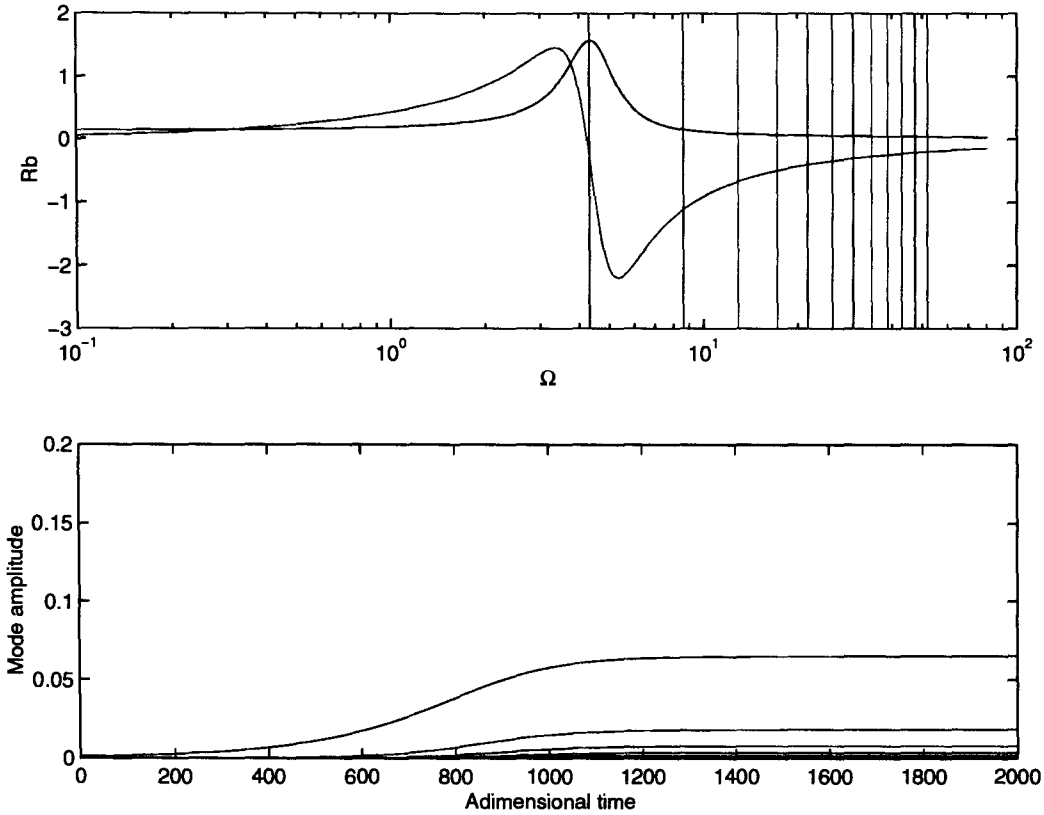

Mode	α_n	ϑ_n	Limit amplitude
1	27.	34.	0.0651
2	-214.	101.	0.0183
3	-452.	117.	0.00786
4	-763.	196.	0.00370
5	-1144.	334.	0.00180
6	-1591.	539.	0.000887
7	-2102.	820.	0.000438
8	-2672.	1186.	0.000216
9	-3299.	1648.	0.000106
10	-3978.	2217.	0.000052
11	-4707.	2903.	0.000025
12	-5481.	3715.	0.000013

FIGURE 3.8. Same R_b as Figure 3.1, but scaled down in amplitude.

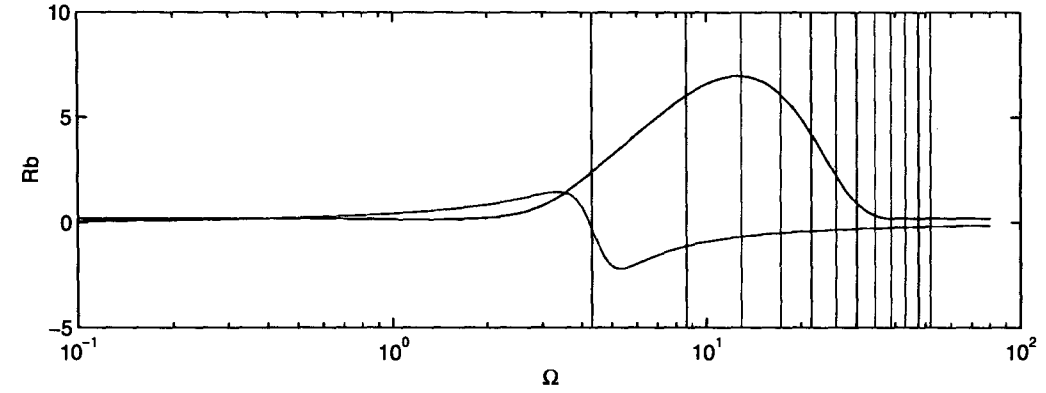

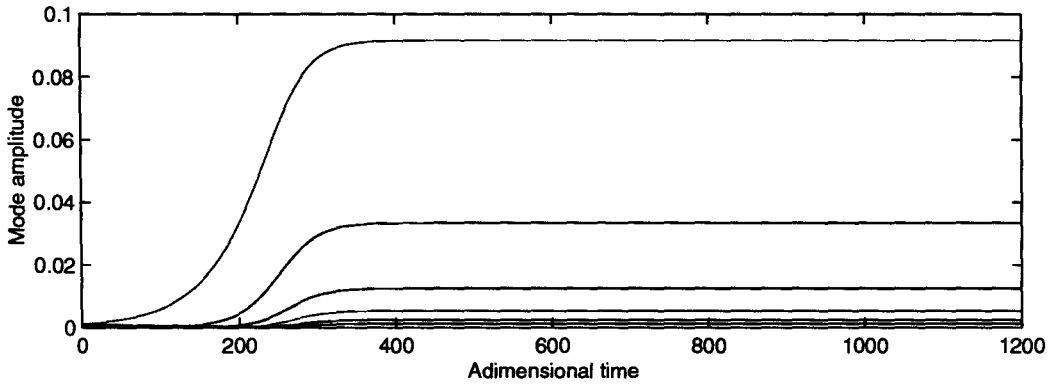

Mode	α_n	ϑ_n	Limit amplitude
1	-26.	34.	0.0
2	101.	101.	0.0916
3	-66.	117.	0.0
4	-446.	196.	0.0334
5	-966.	334.	0.0
6	-1559.	539.	0.0125
7	-2162.	820.	0.0
8	-2772.	1186.	0.00534
9	-3407.	1648.	0.0
10	-4086.	2217.	0.00242
11	-4814.	2903.	0.0
12	-5588.	3715.	0.00116

FIGURE 3.9. *Broad-peak* response function with low amplitude.

Figure 3.8 and Figure 3.9 present the effect of scaling the response function without changing its shape. They should be compared with the results of Figures 3.1 and 3.5: the amplitude of the real part of R_b is reduced by a constant scale factor. The dynamics of the systems are still the same, but the amplitude of the limit cycle is correspondingly diminished. Note that a small reduction of the amplitude for the case of the broad-peak response function causes a sensible reduction of the resulting limit cycle.

4. Modeling the Response Function With Surface and Gas Phase Dynamics

In a solid propellant rocket, the primary chemical activity and the chief sources of energy reside in a thin region adjacent to the solid material. It is the coupling between those processes and unsteady motions in the medium formed by the combustion products that is primarily responsible for most combustion instabilities. For small amplitude motions — 'small' being imprecisely defined — the coupling processes are conveniently represented by *response functions.* A response function is the ratio of the fluctuation of the responding variable and the fluctuation of the variable causing the response. In the present context, either pressure or velocity fluctuations are the causes, and usually the fluctuation of the burning rate is chosen as the responding variable. Here we will be concerned only with the response function for pressure fluctuations, R_b, defined as

$$R_b = \frac{m'/\bar{m}}{p'/\bar{p}} \tag{4.1}$$

Normally both m' and p' stand for steady oscillations. Then R_b is a complex quantity possessing amplitude and phase, or equivalently, real and imaginary parts. That is the situation assumed here, implying at least two deficiencies well-known but sometimes not explicitly noted. First, the definition (4.1) is truly useful only for linear behavior. One can make *ad hoc* adjustments to account for amplitude dependence of R_b, but for investigating nonlinear behavior, it is probably better to follow a different tactic for representing the combustion dynamics. Second, burning surfaces are not perfectly smooth, and most practical propellants are structurally heterogeneous. The use of (4.1) as a boundary condition on oscillations in a chamber therefore implies some sort of averaging (locally) over the surface. The justification, in principle, is that the scale of surface irregularities is exceedingly small compared to the scale (i.e., the wavelength) of organized motions in the chamber.

Concerning the first deficiency, it must be emphasized that the linear boundary condition can be used without approximation to investigation of nonlinear motions within the chamber. No violations of either mathematical or physical principles accompany mixing of linear and nonlinear processes. The second deficiency, however appealing the justification may be, and however accurate the approximation often is, nevertheless excludes 'noisy' or 'stochastic' sources in the combustion zone. Existence of such phenomenon has long been known, but has never, to the authors' knowledge, been investigated in any depth. Possible consequences of such stochastic sources have been addressed in both linear (references [10] – [12]) and nonlinear cases (references [4], [13], [14]), but no detailed realistic models exist for the physical processes.

It is not the intent here to address these matters. Rather, we are concerned with a deficiency of the model commonly used as the basis for computing R_b and for interpreting experimental results, namely the 'QSHOD' model. There are two approaches to constructing explicit formulas for R_b. These have been labelled the Z-N (Zeldovich-Novozhilov) formulation, and the flame model (FM) approach. In practically all analyses based on these approaches, the only dynamics are associated with unsteady heat transfer in the condensed phase. While variations of the basic theme have been studied — including reacting layers within the condensed phase — the dynamics remain essentially unchanged. The significant result is that the characteristic frequency for the unsteady response is hardly affected, being close to $\bar{r}^2/\kappa_c$, where $\bar{r}$ is the linear burning rate and κ_c is the thermal diffusivity of the condensed phase. Hence the response function has a single, rather broad peak,

typically in the range of a few hundred up to perhaps a thousand hertz. An example is shown in Figure 4.1, for $A = 6$, $B = 0.55$, and $\tau_d = 0$ in the formula (4.2) for R_b. There is considerable experimental evidence suggesting that the response functions for real propellants often are noticeably larger at higher frequencies than predicted by these theories. That is the matter addressed here.

It seems that the most logical prospect for producing higher response at higher frequencies is dynamical heat transfer in the gas phase. The 'QS' in 'QSHOD' stands for 'quasi-steady,' referring to the behavior of the gas phase. At least four works (references [15] – [18]) have been devoted to relaxing that constraint. Here we treat the same problems with a simplified model to try to clarify the extent to which the process in question may be a significant contribution in practice.

A second appealing process, or class of processes, accompanies the complicated behavior in the region immediately adjacent to the interface of the condensed phase, where solid material is converted to gas, or liquid, or 'foam,' or a mixture of gas and condensed species. High-speed films have long suggested that the dynamics of this region may well affect the response significantly. This zone is particularly interesting because the very complicated processes may be quite sensitive to small changes of propellant composition. For example, the sizes of aluminum agglomerates on the surface of a metallized propellant seem to be strongly influenced by small amounts of impurities, including aluminum oxide itself (A. Babuk, private communication, June 1998).

The model constructed and analyzed here is intentionally simple. Structural simplicity is required if one is to obtain results without elaborate numerical simulations, to assess as directly as possible whether or not the dynamical processes described do indeed merit more thorough analysis. Thus we are concerned essentially with phenomenological modeling carried far enough to produce approximate but quantitative results for the response function.

Recently, Novozhilov (private communication, May 1998) reported a result for R_b incorporating a pure time delay τ_d associated with conversion of condensed material to gaseous (or liquid) products at the interface. In terms of the A–B formula (references [9] and [19]), Novozhilov finds that the parameter A is unchanged but B is replaced by $Be^{-i\omega\tau_d}$:

$$R_b = \frac{nABe^{-i\omega\tau_d}}{\lambda_c + \frac{A}{\lambda_c} - (A+1) + ABe^{-i\omega\tau_d}} \tag{4.2}$$

Figure 4.1 shows some results computed with (4.2). Although there is a pleasing, though small, effect in the vicinity of the peak of the real part, if τ_d is given an appropriate value, the behavior at higher frequencies is unacceptable. Rapid oscillations will always occur in a response function containing a pure *constant* delay, because for sufficiently large ω, the phase $\omega\tau_d$ changes rapidly. Only if the delay is a rapidly decreasing function of frequency will this behavior not arise. Note that any response function can be expressed in terms of a time delay by writing

$$R_b = R_b^{(r)} + iR_b^{(i)} = |R_b|e^{i\phi} \tag{4.3}$$

where $|R_b| = [(R_b^r)^2 + (R_b^i)^2]^{1/2}$ and $\phi = \omega\tau = \tan^{-1}(R_b^i/R_b^r)$. Hence $\tau = \omega^{-1}\tan^{-1}(R_b^i/R_b^r)$ is a function of frequency which for the A–B form (4.2) tends rapidly to zero when $\tau_d = 0$ in (4.2).

It seems that by its very nature, the Z-N approach cannot be used to investigate the dynamics we wish to consider here. Novozhilov [18] introduced the dynamics of the gas phase with a flame sheet model of combustion and hence departs from the traditional Z-N approach. He also gives a good review of previous calculations for this problem, including critical comments concerning the results of [16]. With the flame sheet model, the results are similar to those attained by Clavin and Lazemi [17]. Novozhilov's paper deserves closer attention, but the copy available to the authors at this has very poor quality and is partly unreadable.

In this work we wish to accommodate possible dynamics both of the region near the surface and in the gas phase. We therefore base our analysis on the explicit model shown in Figure 4.2. The analysis is an elaboration of that outlined in [19], extended to include approximations to the

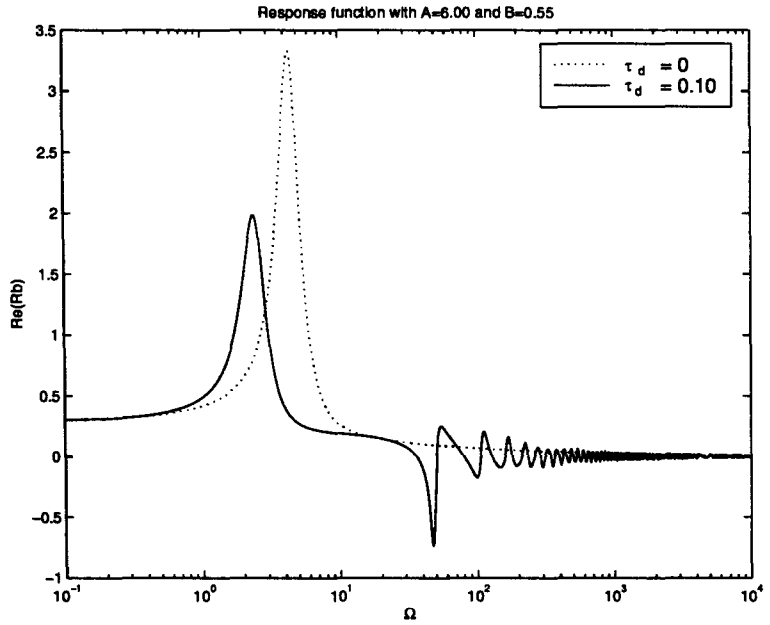

FIGURE 4.1. Plot of the response function with and without time delay.

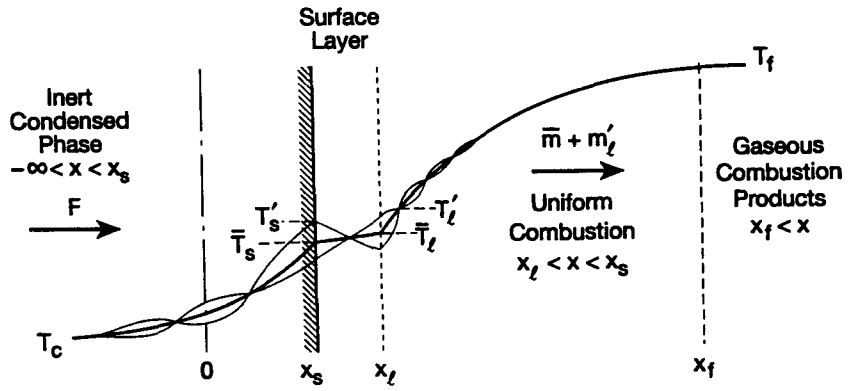

FIGURE 4.2. The model investigated here.

dynamics of the two regions, the surface layer $x_s < x < x_l$ and the gas phase $x_l < x < x_f$. The procedure is straightforward: solve suitable equations for the temperature fluctuations in the three zones and match at the two planes x_s and x_l. The presence of unsteady flow is the chief complication, causing fluctuations of x_s and x_l which must be taken into account. In that connection, we make two serious approximations:

(i) the dynamics of the surface layer is not analyzed, but represented by transfer functions;
(ii) the mass flow in the gas phase ($x_l < x < x_f$) responds quasi-statically, oscillating as a 'plug flow' so the fluctuations m' of the mass flux m are in phase throughout the zone.

It is important that the approximation (ii) does *not* exclude true thermal dynamics. The reason is, roughly, that fluctuations of the mass flow propagate with the speed of sound, while temperature fluctuations propagate with a speed reflecting the presence of both heat conduction and convection.

Because the origin of coordinates, Figure 4.2, is fixed to the average position of the interface, the actual interface oscillates about that position. The plane x_l oscillates about its average position $\bar{x}_l$ which, because it is tied to the interface x_s, also oscillates with respect to the origin, although its average position is non-zero. These motions, complicated in general, cause computational difficulty because the matching conditions must consequently be satisfied on the moving planes x_s and x_l. However, in the limit of small-amplitude linearized motions, the difficulties are all overcome by referring the conditions to the fixed plane $x = 0$, using Taylor-series expansions.

4.1. **Unsteady Heat Transfer at the Interface of the Condensed Phase.** In the coordinate system defined in Figure 4.2, the energy equation written for the temperature in the condensed phase is

$$\rho_c c \frac{\partial T}{\partial t} + \rho_c \bar{r} c \frac{\partial T}{\partial x} = k_c \frac{\partial^2 T}{\partial x^2} \tag{4.4}$$

We assume throughout that the specific heat c and thermal conductivity k_c are constant. For small-amplitude motions, the temperature is split into the sum of its average value $\bar{T}$, independent of time, and the fluctuation T', asserted to be much smaller than T. Define the dimensionless coordinate

$$\xi_c = \left(\frac{\bar{m}c}{\kappa_c}\right) x = \left(\frac{\bar{r}}{\kappa_c}\right) x \tag{4.5}$$

where κ_c is the thermal diffusivity. The solutions to 4.4 for $\bar{T}$ and T' are

$$\frac{\bar{T} - \bar{T}_c}{\bar{T}_s - T_c} = e^{\xi_c} \tag{4.6}$$

$$T' = T'_0 e^{\lambda_c \xi_c} = \hat{T}_0 e^{i\Omega_c \tau} e^{\lambda_c \xi_c} \tag{4.7}$$

The dimensionless frequency is

$$\Omega_c = \left(\frac{\kappa_c}{\bar{r}^2}\right) \omega \tag{4.8}$$

and λ_c is the solution to

$$\lambda_c(\lambda_c - 1) = i\Omega_c \tag{4.9}$$

Choosing the sign on the radical to ensure that the temperature fluctuations decay for $x \to -\infty$, we have the real and imaginary parts of λ_c:

$$\lambda_c^{(r)} = \frac{1}{2}\left\{1 + \frac{1}{\sqrt{2}}\left[\sqrt{1 + 16\Omega_c^2} + 1\right]^{1/2}\right\} \qquad (a)$$

$$\lambda_c^{(i)} = \frac{1}{2\sqrt{2}}\left[\sqrt{1 + 16\Omega_c^2} - 1\right]^{1/2} \qquad (b) \tag{4.10}$$

The formula (4.7) applies only to the region $\xi_c \leq 0$. To obtain the solution valid up to the interface at x_s, we expand in Taylor series,

$$T'_s = T'_0 + x_s \left(\frac{d\bar{T}}{dx}\right)_{0\pm} = T'_0 + \xi_{cs} \left(\frac{d\bar{T}}{d\xi_c}\right)_{0\pm} \qquad (a)$$

$$\left(\frac{\partial T'}{\partial x}\right)_{s\pm} = \left(\frac{\partial T'}{\partial x}\right)_{0\pm} + x_s \left(\frac{d^2\bar{T}}{dx^2}\right)_{0\pm} \qquad (b) \qquad (4.11)$$

where the subscripts $(\ )_\pm$ refer to the upstream $(-)$ or downstream $(+)$ sides of the origin or interface. In the variable ξ_c, (4.11)a is

$$\left(\frac{\partial T'}{\partial \xi_c}\right)_{s\pm} = \left(\frac{\partial T'}{\partial \xi_c}\right)_{0\pm} + \xi_{sc} \left(\frac{d^2\bar{T}}{d\xi_c^2}\right)_{0\pm} \qquad (4.12)$$

A formula for the displacement x_s of the interface is found by applying the principle of conservation of mass relative to the interface, written in the reference frame in which the condensed phase moves with the constant speed $\bar{r}$:

$$\rho_c(\bar{r} - \dot{x}_s) = \rho_{s+}(u_{s+} - \dot{x}_s) = \rho_{ls}(u_{ls} - \dot{x}_s) \qquad (4.13)$$

where ρ_{s+}, u_{s+} refer to the material on the downstream side of the interface, here identified by the subscript $(\ )_l$, ("liquid"), whatever may be the actual state of the stuff. With time dependence $e^{i\omega t}$, (4.13) gives

$$\xi_{cs} = -\frac{1}{i\Omega_c} \frac{\rho_c}{\hat{\rho}_c} \frac{m'_s}{\bar{m}} \qquad (4.14)$$

where

$$\hat{\rho}_c = \rho_c \left(1 - \frac{\bar{\rho}_{ls}}{\rho_c}\right) \qquad (4.15)$$

Combination of (4.6), (4.7), (4.12), and (4.14) gives the result for unsteady heat transfer into the condensed phase:

$$\frac{1}{\bar{m}_c} \left[k_c \frac{\partial T'}{\partial x}\right]_{s-} = \lambda_c T'_s + \frac{\bar{T}_s - T_c}{\lambda_c} \frac{\rho_c}{\hat{\rho}_c} \frac{m'_s}{\bar{m}} \qquad (4.16)$$

The heat transfer required to sustain the motion implied by T'_s and $m_s/\bar{m}$ must be supplied from the downstream side of the interface. Application of the principle of conservation of energy to a small control volume enclosing the interface gives

$$\rho_c(\bar{r} - \dot{x}_s)k_{s-} + \left[k_l \frac{\partial T}{\partial x}\right]_{s+} = \rho_{ls}(u_{ls} - \dot{x}_s)k_s + \left[k_c \frac{\partial T}{\partial x}\right]_{s-} \qquad (4.17)$$

After substitution of (4.6), the steady form of (4.17) is

$$\frac{1}{\bar{m}_c} \left[k_l \frac{d\bar{T}}{dx}\right]_{s+} = (\bar{T}_s - T_c) + L_s \qquad (4.18)$$

where $L_s = h_{s+} - h_{s-}$ is the latent heat for the surface reaction, having positive sign for an endothermic process. The unsteady form of (4.17) is

$$\left[k_l \frac{\partial T'}{\partial x}\right]_{s+} = \left[k_c \frac{\partial T'}{\partial x}\right]_{s-} + m'_s \bar{L}_s + \bar{m}(c_p - c)T'_s \qquad (4.19)$$

Substitution of (4.16) leads to

$$\frac{1}{\bar{m}c} \left[k_l \frac{\partial T'}{\partial x}\right]_{s+} = \lambda_c T'_s + \left(\frac{c_p}{c} - 1\right) T'_s + \left[\frac{\rho_c}{\hat{\rho}_c} \frac{\bar{T}_s - T_c}{\lambda_c} + \frac{\bar{L}_s}{c}\right] \frac{m'_s}{\bar{m}} \qquad (4.20)$$

We adopt the common practice of using a law of the Arrhenius form to represent the phase changes at the interface:

$$m_s = B_s p^{n_s} T_s^{\alpha_s} e^{-E/R_0 T_s} \tag{4.21}$$

Thus in the linearized limit, the fluctuation of mass flux is

$$\frac{m_s'}{\bar{m}} = E_s \frac{T_s'}{\bar{T}_s} + n_s \frac{p'}{p} \tag{4.22}$$

where $E_s = \alpha_s + E/R_0 \bar{T}_s$. Note that one could insert a phase factor $e^{i\phi}$ in the terms on the right-hand side of (4.22) to represent delays in the conversion process. Later assumptions here will effectively include that sort of dynamics. Substituting (4.22) in (4.19) we obtain the formula for the heat transfer from the downstream side of the interface,

$$\frac{1}{\bar{m}c}\left[k_l \frac{\partial}{\partial x}\left(\frac{T'}{\bar{T}_s}\right)\right]_{l+} = \left(\lambda_c + \frac{A}{\lambda_c}\right)\frac{T_s'}{\bar{T}_s} + \mathcal{H}_s \frac{T_s'}{\bar{T}_s} + n_s\left(L + \frac{\Delta T_s}{\lambda_c}\right)\frac{p'}{\bar{p}} \tag{4.23}$$

where

$$\begin{aligned} A &= \frac{\rho_c}{\hat{\rho}_c} E_s \left(1 - \frac{T_c}{\bar{T}_s}\right) && (a) \\ \mathcal{H}_s &= \frac{L_s E_s}{c\bar{T}_s} + \left(\frac{c_p}{c} - 1\right) && (b) \\ L &= \frac{L_s}{c\bar{T}_s} && (c) \\ \Delta T_s &= \frac{\rho_c}{\hat{\rho}_c}\left(1 - \frac{T_c}{\bar{T}_s}\right) && (d) \end{aligned} \tag{4.24}$$

The right-hand side of (4.23) contains the dynamics of the thermal wave in the condensed phase, and unsteady conversion of material at the interface. In the Z-N formulation of the response function, the left-hand side is inferred from experimental data by applying an assumption of quasi-steady behavior of the processes downstream of the interface. Here we construct a phenomenological representation of the dynamics of that region.

4.2. **Dynamics of the Surface Layer and the Gas Phase.** In this work we will not attempt detailed analysis of the surface layer extending in the space $x_s < x < x_l$. Rather, we will represent the dynamics of that zone in *ad hoc* fashion by introducing transfer functions $T_l(\omega)$, $M_l(\omega)$, and $Q_l(\omega)$ connecting fluctuations of mass flux, temperature, and heat transfer at the edges of the zone:

$$\begin{aligned} \frac{m_l'}{\bar{m}} &= M_l(\omega)\frac{m_s'}{\bar{m}} && (a) \\ \frac{T_l'}{\bar{T}_l} &= T_l(\omega)\frac{T_s'}{\bar{T}_s} && (b) \\ \frac{1}{\bar{m}c_p}\left[k_g \frac{\partial}{\partial x}\left(\frac{T'}{\bar{T}_l}\right)\right]_l &= \frac{Q_l}{\bar{m}c}\left[k_l \frac{\partial}{\partial x}\left(\frac{T'}{\bar{T}_s}\right)\right]_{s+} && (c) \end{aligned} \tag{4.25}$$

We assume that medium is largely gaseous at the downstream edge of the surface layer, so the thermal conductivity is denoted by k_g.

Moreover, we assume quasi-steady behavior of the mass flow in the region downstream of the interface; in particular, $m_l' = m_s'$. In some sense, then, the location x_l of the downstream edge of the surface layer follows the location x_s of the interface; i.e., it seems a reasonable assumption that

$\dot{x}_l = \dot{x}_s$, implying

$$x_l = \frac{k_c}{\bar{m}c}\xi_{cs} = -\frac{k_c}{\bar{m}c}\frac{1}{i\Omega_c}\frac{\rho_c}{\hat{\rho}_c}\frac{m_s'}{\bar{m}} \tag{4.26}$$

It is more appropriate to make x_l dimensionless with parameters identifying the gas phase, so analogous to (4.5), we define

$$\xi_g = \frac{\bar{m}c_p}{k_g}x = \frac{\bar{u}_b}{\kappa_g}x \tag{4.27}$$

where

$$\kappa_g = \frac{k_g}{\bar{\rho}_g c_p} \tag{4.28}$$

and $\bar{u}_b$ is the velocity of the products departing the combustion zone. Thus the dimensionless frequency is

$$\Omega_g = \left(\frac{\kappa_g}{\bar{u}_b^2}\right)\omega \tag{4.29}$$

and (4.26) can be written

$$\xi_{gl} = -\left(\frac{\bar{r}}{\bar{u}_b}\right)\left(\frac{\rho_c}{\hat{\rho}_c}\right)\frac{1}{i\Omega_g}\frac{m_s'}{\bar{m}} \tag{4.30}$$

Dynamical behavior of the layer may also be accommodated here by introducing a transfer function X_l which for simpler writing we define to include the factors $(\bar{r}/\bar{u}_b)(\rho_c/\hat{\rho}_c)$:

$$\xi_{gl} = -\frac{1}{i\Omega_g}X_l\frac{m_s'}{\bar{m}} \tag{4.31}$$

4.2.1. *Mean Temperature Distribution.* The energy equation written for temperature is the gas phase is

$$\rho_g c_p\frac{\partial T}{\partial t} + \rho_g u_g c_p\frac{\partial T}{\partial x} = k_g\frac{\partial^2 T}{\partial x^2} + Q_f w \tag{4.32}$$

Hence the equation for the mean and fluctuating temperatures are

$$\bar{m}c_p\frac{d\bar{T}}{dx} = k_g\frac{d^2\bar{T}}{dx^2} + Q_f\bar{w} \tag{4.33}$$

Easy solution to this equation is blocked in general because the reaction rate $\bar{w}$ is a nonlinear function of temperature, for example the Arrhenius function. We avoid the problem entirely by supposing that the combustion is uniform in space, extending from some location x_i of ignition to the downstream edge x_f of the flame. To simplify the model further, we take $x_i = x_l$: burning begins immediately at the downstream edge of the surface layer. The first integral of (4.33) is

$$k_g\left(\frac{d\bar{T}}{dx}\right)_{l+} = \bar{m}\left[Q_f - c_p(\bar{T}_f - \bar{T}_l)\right] \tag{4.34}$$

which is a fairly evident statement of the power balance across the layer. We assume always that k_g and c_p are constant and we used the relation

$$\bar{m} = \int_{x_i}^{x_f}\bar{w}dx \tag{4.35}$$

Now define the variable $\zeta = e^{\xi_g}$ and (4.33) can be written

$$-\zeta^2\frac{d^2}{d\zeta^2}\left(\frac{\bar{T}}{\bar{T}_l}\right) = \Lambda^2 \tag{4.36}$$

with

$$\Lambda^2 = \frac{Q_f k_g \bar{w}}{\bar{m}^2 c_p^2 \bar{T}_l} \tag{4.37}$$

The solution to (4.36)

$$\frac{\bar{T}}{\bar{T}_l} = \frac{\bar{T}_f}{\bar{T}_l} - \Lambda^2 \left[\ln \frac{\zeta_f}{\zeta} - \left(1 - \frac{\zeta}{\zeta_f} \right) \right] \qquad (\bar{\zeta}_l < \zeta < \bar{\zeta}_f) \tag{4.38}$$

To this point, the value of Λ^2, the eigenvalue for this problem, is unknown and must be found by satisfying the various boundary and matching conditions. The result is

$$\Lambda^2 = \frac{\left(\frac{\bar{T}_f}{\bar{T}_l} - 1 \right)}{\ln \frac{\zeta_f}{\zeta_l} - \left(1 - \frac{\zeta_l}{\zeta_f} \right)} \tag{4.39}$$

which requires specification of ζ_l. Finally, the thickness ζ_f of the flame can be computed from

$$\frac{\bar{\zeta}_f}{\bar{\zeta}_l} = 1 + \left[1 - \frac{c_p(\bar{T}_f - \bar{T}_l)}{Q_f} \right] \ln \frac{\bar{\zeta}_f}{\bar{\zeta}_l} \tag{4.40}$$

Additional details may be found in reference [19] for the case in which the surface layer is absent. The main point here is that explicit solution can be found for the temperature profile if the combustion is uniform and k_g, c_p are assumed constant. In terms of ξ_g, (4.38) is

$$\frac{\bar{T}}{\bar{T}_l} = \frac{\bar{T}_f}{\bar{T}_l} - \Lambda^2 \left[(\bar{\xi}_{gf} - \xi_g) - (1 - f e^{\xi_g}) \right] \tag{4.41}$$

where

$$f = e^{-\xi_{gf}} \tag{4.42}$$

We will need later the first and second derivatives of (4.41)

$$\begin{aligned} \frac{d}{d\xi_g}\left(\frac{\bar{T}}{\bar{T}_l} \right) &= \Lambda^2 \left(1 - f e^{\xi_g} \right) && (a) \\ \frac{d^2}{d\xi_g^2}\left(\frac{\bar{T}}{\bar{T}_l} \right) &= -\Lambda^2 f e^{\xi_g} && (b) \end{aligned} \tag{4.43}$$

4.2.2. *Unsteady Temperature Distribution.* Written for the temperature fluctuation, equation (4.32) becomes

$$i\Omega_g \tau' + \frac{\partial \tau'}{\partial \xi_g} - \frac{\partial^2 \tau'}{\partial \xi_g^2} = -\frac{m_l'}{\bar{m}} \frac{d\bar{\tau}}{d\xi_g} + \Lambda^2 \frac{w'}{\bar{w}} \tag{4.44}$$

where $\tau = T/\bar{T}_l$ and the assumption of quasi-steady behavior of the mass flux requires $m' = m_l'$ for $x > x_l$. It is reasonable to assume that because the presence is uniform throughout a low-speed flame, then for the case of w uniform, we may assume that changes in the reaction rate may be related to changes of pressure: $w' \sim p'$. We set $w'/\bar{w} = W(p'/\bar{p})$ and with (4.43)a, equation (4.44) is

$$i\Omega_g \tau' + \frac{\partial \tau'}{\partial \xi_g} - \frac{\partial^2 \tau'}{\partial \xi_g^2} = -\Lambda^2 \left(1 + f e^{\xi_g} \right) \frac{m_l'}{\bar{m}} + \Lambda^2 w \frac{p'}{\bar{p}} \tag{4.45}$$

A particular solution to this equation is

$$\tau_p' = \frac{1}{i\Omega_g} \left[c_1 + c_2 e^{\xi_g} \right] \tag{4.46}$$

with

$$c_1 = -\Lambda^2 \left(\frac{m_l'}{\bar{m}} - w \frac{p'}{\bar{p}} \right) \qquad (a)$$
$$c_2 = -\Lambda^2 f \frac{m_l'}{\bar{m}} \qquad (b) \tag{4.47}$$

The homogeneous solution is $\tau_1 e^{\lambda_{g_1} \xi_g} + \tau_2 e^{\lambda_{g_2} \xi_g}$ where λ_{g_1} and λ_{g_2} are the two solutions to

$$\lambda_g^2 - \lambda_g - i\Omega_g = 0 \tag{4.48}$$

Hence the general solution of (4.45) is

$$\tau' = \tau_1 e^{\lambda_{g_1} \xi_g} + \tau_2 e^{\lambda_{g_2} \xi_g} + \frac{1}{i\Omega_g} \left(c_1 + c_2 f e^{\xi_g} \right) \tag{4.49}$$

and its derivatives are

$$\frac{\partial \tau'}{\partial \xi_g} = \lambda_{g_1} \tau_1 e^{\lambda_{g_1} \xi_g} + \lambda_{g_2} \tau_2 e^{\lambda_{g_2} \xi_g} + \frac{c_2 f}{i\Omega_g} e^{\xi_g} \qquad (a)$$
$$\frac{\partial^2 \tau'}{\partial \xi_g^2} = \lambda_{g_1}^2 \tau_1 e^{\lambda_{g_1} \xi_g} + \lambda_{g_2}^2 \tau_2 e^{\lambda_{g_2} \xi_g} + \frac{c_2 f}{i\Omega_g} e^{\xi_g} \qquad (b) \tag{4.50}$$

Because we will use the solution to determine formulas for the temperature and heat transfer fluctuation at the edge of the surface layer, we evaluate τ_1 and τ_2 by satisfying the boundary condition at the average position of the downstream edge of the flame:

$$\tau' = \tau_{\bar{f}}' \qquad (a)$$
$$\frac{\partial \tau'}{\partial \xi_g} = q_{\bar{f}}' \qquad (\xi_f = \bar{\xi}_f) \qquad (b) \tag{4.51}$$

The results are

$$\tau_1 = \frac{e^{\lambda_{g_1} \bar{\xi}_{gf}} (\lambda_{g2} \kappa_1 - \kappa_2)}{\lambda_2 - \lambda_1} \qquad (a)$$
$$\tau_2 = \frac{e^{\lambda_{g_2} \bar{\xi}_{gf}} (\kappa_2 - \lambda_{g1} \kappa_1)}{\lambda_2 - \lambda_1} \qquad (b) \tag{4.52}$$

and

$$\kappa_1 = \tau_{\bar{f}}' - \frac{1}{i\Omega_g} (c_1 + c_2) \qquad (a)$$
$$\kappa_2 = q_{\bar{f}}' - \frac{c_2}{i\Omega_g} \qquad (b) \tag{4.53}$$

The solution for the fluctuating temperature and heat transfer in the gas phase is:

$$\begin{aligned}\frac{T'}{\bar{T}_l} &= \frac{T'_{\bar{f}}}{\bar{T}_l}\frac{1}{\Delta\lambda}\left[\lambda_{g2}e^{-\lambda_{g1}(\bar{\xi}_{gf}-\xi_g)} - \lambda_{g1}e^{-\lambda_{g2}(\bar{\xi}_{gf}-\xi_g)}\right] \\ &+ \frac{c_1}{i\Omega}\left[1 - \frac{1}{\Delta\lambda}\left\{\lambda_{g2}e^{-\lambda_{g1}(\bar{\xi}_{gf}-\xi_g)} - \lambda_{g1}e^{-\lambda_{g2}(\bar{\xi}_{gf}-\xi_g)}\right\}\right] \\ &+ c_2\left[\frac{1}{i\Omega}e^{-(\bar{\xi}_{gf}-\xi_g)} + \frac{1}{\Delta\lambda}\left\{\frac{1}{\lambda_{g1}}e^{-\lambda_{g2}(\bar{\xi}_{gf}-\xi_g)} - \frac{1}{\lambda_{g2}}e^{-\lambda_{g1}(\bar{\xi}_{gf}-\xi_g)}\right\}\right] \\ &+ q'_{\bar{f}}\frac{1}{\Delta\lambda}\left[e^{-\lambda_{g1}(\bar{\xi}_{gf}-\xi_g)} - e^{-\lambda_{g2}(\bar{\xi}_{gf}-\xi_g)}\right] \qquad (a)\end{aligned} \tag{4.54}$$

$$\begin{aligned}\frac{\partial}{\partial\xi_g}\frac{T'}{\bar{T}_l} &= T'_{\bar{f}}\frac{i\Omega}{\Delta\lambda}\left[e^{-\lambda_{g2}(\bar{\xi}_{gf}-\xi_g)} - e^{-\lambda_{g1}(\bar{\xi}_{gf}-\xi_g)}\right] \\ &+ \frac{c_1}{\Delta\lambda}\left[e^{-\lambda_{g1}(\bar{\xi}_{gf}-\xi_g)} - e^{-\lambda_{g2}(\bar{\xi}_{gf}-\xi_g)}\right] \\ &+ c_2\left[\frac{1}{i\Omega}e^{-(\bar{\xi}_{gf}-\xi_g)} + \frac{1}{\Delta\lambda}\left\{\frac{\lambda_{g2}}{\lambda_{g1}}e^{-\lambda_{g2}(\bar{\xi}_{gf}-\xi_g)} - \frac{\lambda_{g1}}{\lambda_{g2}}e^{-\lambda_{g1}(\bar{\xi}_{gf}-\xi_g)}\right\}\right] \\ &+ q'_{\bar{f}}\frac{1}{\Delta\lambda}\left[\lambda_{g1}e^{-\lambda_{g2}(\bar{\xi}_{gf}-\xi_g)} - \lambda_{g2}e^{-\lambda_{g1}(\bar{\xi}_{gf}-\xi_g)}\right] \qquad (b)\end{aligned}$$

In several places, we have used the properties of equation (4.48) for λ_g that $\lambda_{g1}\lambda_{g2} = -i\Omega_g$; note also that $\lambda_{g1} + \lambda_{g2} = -1$, and $\Delta\lambda = \lambda_2 - \lambda_1$.

Despite the appearance of the frequency Ω_g in the denominator, in several places, (4.2.2)a, b both are finite for $\Omega_g \to 0$, the quasi-static limit:

$$\begin{aligned}\frac{T'}{\bar{T}_l} &\to \tau'_{\bar{f}} + q'_{\bar{f}}\left(1 - e^{-\chi}\right) - \Lambda^2\frac{w'}{\bar{w}}\left(\chi - 1 + e^{-\chi}\right) - \Lambda^2\frac{m'}{\bar{m}}\left[e^{-\chi}(1+\chi) - \chi\right] \qquad (a) \\ \frac{\partial}{\partial\xi_g}\left(\frac{T'}{\bar{T}_g}\right) &\to q'_{\bar{f}}e^{-\chi} + \Lambda^2\frac{w'}{\bar{w}}\left(1 - e^{-\chi}\right) - \Lambda^2\frac{m'}{\bar{m}}\left[\chi e^{-\chi}\right] \qquad (b)\end{aligned} \tag{4.55}$$

where

$$\chi = \bar{\xi}_{gf} - \xi_g \tag{4.56}$$

At the downstream edge of the flame, the heat transfer q'_f is zero always, a condition that is imposed by applying the Taylor series expansion about the mean position $\bar{\xi}_{gf}$:

$$q'_f = \left[\frac{\partial}{\partial\xi_g}\left(\frac{T'}{\bar{T}_l}\right)\right]_f = \left[\frac{\partial}{\partial\xi_g}\left(\frac{T'}{\bar{T}_l}\right)\right]_{\bar{f}} + \xi'_{gf}\left[\frac{d^2}{d\xi_g^2}\left(\frac{\bar{T}}{\bar{T}_l}\right)\right]_{\bar{f}} = 0 \tag{4.57}$$

so

$$\left[\frac{\partial}{\partial\xi_g}\left(\frac{T'}{\bar{T}_l}\right)\right]_{\bar{f}} = q'_{\bar{f}} = -\xi'_{gf}\left[\frac{d^2}{d\xi_g^2}\left(\frac{\bar{T}}{\bar{T}_l}\right)\right]_{\bar{f}} \tag{4.58}$$

That is, the fluctuation of heat transfer at the mean position of the flame edge is associated with the fluctuation ξ'_{gf} of the flame thickness.

To complete the analysis, formal statements must be made about the fluctuations of the surfaces ξ'_{gl} and ξ'_{gf} of the edges of the combustion zone in the gas phase; and models of the surface layer must be constructed to give the transfer functions $M_l(\omega)$, $T_l(\omega)$, and $Q_l(\omega)$ in (4.25)a, b, c. Those tasks remain.

We should emphasize particularly the possibilities offered by including the surface layer in this model. Innumerable observations have shown the extraordinarily complicated behavior that exists

in this region, arising especially from the heterogeneous character of the condensed material. Those processes, including, notably, the formation, agglomeration, and ignition of liquid aluminum drops at the surface of metallized propellants, have yet to be incorporated in analysis of the response function. The scheme described here can accommodate those dynamics; the most difficult aspect is constructing an appropriate model.

The spatial and temporal statistical character of a burning propellant can also be treated within this framework. This is an interesting problem to investigate as a possible origin of stochastic noise sources in a solid propellant rocket combustor. We have cited, in remarks following equation (4.1), works treating some global dynamical consequences of noise sources, but the detailed physical processes responsible have not been analyzed. There are roughly two classes of noise sources in a solid rocket: turbulent flow within the volume of the chamber; and surface processes. In view of existing works and experience with noise generated by turbulence and combustion, it seems most likely that those sources dominate. However, the surface processes merit investigation at least to assess their relative importance.

5. Concluding Remarks

One of the purposes of this paper is to explain, with illustrative examples, some aspects of the strategy followed in the Caltech MURI program. This is by no means a thorough summary of the program, but does serve to emphasize the central importance of the response function as a vehicle for capturing the combustion dynamics of a burning propellant. Constructing a realistic and useful response function is a matter of combining modelling of the dominant physical processes with measurements of the response function, not discussed here. Thus that function serves as the primary connection between Tasks 2 and 3, as shown in Figure 1.1, and provides the principal information required of Task 2 to carry out analyses under Task 3. The discussion here is far from a complete description of current work in the MURI program. In particular, there are extensive experimental and modelling efforts not mentioned; and in parallel with the approximate form of analysis reviewed here in Sections 2 and 3, there are several important works involving extensive numerical simulations. Those subjects, and the topics treated briefly here, will be thoroughly carried out in subsequent publications.

Acknowledgement

This work was sponsored partly by the California Institute of Technology and partly by the Caltech Multidisciplinary University Research Initiative under ONR Grant No. N00014-95-1-1338, Program Manager Dr. Judah Goldwasser.

References

[1] Culick, F.E.C. (1976) Nonlinear behavior of acoustic waves in combustion chambers, Parts I and II. *Astronautica Acta,* **3**, 714–757.

[2] Culick, F.E.C. and Yang, V. (1992) Prediction of the stability of unsteady motions in solid propellant rocket motors. In: *Nonsteady Burning and Combustion Stability of Solid Propellants, Progress in Astronautics and Aeronautics*, **143**, 719–779.

[3] Jahnke, C. and Culick, F.E.C. (1994) An application of dynamical systems theory to nonlinear combustion instabilities. AIAA 31st Aerospace Sciences Meeting (1993), AIAA Paper No. 93-0114. Published in *Journal of Propulsion and Power*, **10**, No. 4, 508–517.

[4] Burnley, V.S. (1996) *Nonlinear Combustion Instabilities and Stochastic Sources.* Ph.D. Thesis, Department of Aeronautics, California Institute of Technology.

[5] Zinn, B.T. and Powell, E.A. (1970) Nonlinear combustion instability in liquid-propellant rocket engines. In: *Thirteenth Symposium (International) on Combustion*, Salt Lake City, Utah.

[6] Powell, E.A. (1970) *Nonlinear Combustion Instability in Liquid-Propellant Rocket Engines.* Ph.D. Thesis, Georgia Institute of Technology, GITAER 70-6.

[7] Zinn, B.T. and Powell, E.A. (1970) Application of the Galerkin method in the solution of combustion-instability problems. *XIXth International Astronautical Congress*, **3**, 59–73.
[8] Powell, E.A. and Zinn, B.T. (1971) A single mode approximation in the solution of nonlinear combustion instability problems. *Combustion Science and Technology*, **3**, 121–132.
[9] Denison, M.R. and Baum, E. (1961) A simplified model of unstable burning of a solid propellant. *ARS J.*, **31**, No. 5, 1112.
[10] Hessler, R.O. (1982) Forced oscillation prediction. In: *20th JANNAF Combustion Meeting.*
[11] Deur, J.M. and Hessler, R.O. (1983) Forced oscillation theory and applications. In: *20th JANNAF Combustion Meeting.*
[12] Deur, J.M. and Hessler, R.O. (1984) Forced oscillation theory. In: *20th AIAA/SAE/ASME Joint Propulsion Conference*, AIAA Paper No. 84-1365.
[13] Burnley, V.S. and Culick, F.E.C. (1998) The influence of combustion noise in acoustic instabilities. *AIAA Journal*, accepted for publication.
[14] Culick, F.E.C., Paparizos, L., Sterling, J., and Burnley, V. (1991) Combustion noise and combustion instabilities in propulsion systems. In: *AGARD Conference on Combat Aircraft Noise* (Conference Proceedings), 515.
[15] Cheng, S.-I. (1954) High-frequency combustion instability in solid propellant rockets. *ARS Journal*, Part I, 27–32; Part II, 103–109.
[16] T'ien, J.S. (1972) Oscillatory burning of solid propellants including gas phase time lag. *Combustion Science and Technology*, **5**, 47–54.
[17] Clavin, P. and Lazemi, D. (1992) Theoretical analysis of oscillatory burning of homogeneous solid propellant including non-steady gas phase effects. *Combustion Science and Technology*, **83**, 1–32.
[18] Novozhilov, B.V. (1993) Acoustic admittance of the surface of burning condensed matter. *Soviet Journal of Chemical Physics,* **10**, No. 11, 2363–2384.
[19] Culick, F.E.C. (1968) A review of calculations for unsteady burning of a solid propellant. *AIAA Journal*, **6**, No. 12.
[20] Culick, F.E.C. and Dehority, G. (1969) An elementary calculation for the burning rate of composite solid propellants. *Combustion Science and Technology*, **1**, No. 3 193–204.
[21] Awad, E. and Culick, F.E.C. (1986) On the existence and stability of limit cycles for longitudinal acoustic modes in a combustion chamber. *Combustion Science and Technology*, **46**, 195–222.
[22] Burnley, V.S. and Culick, F.E.C. (1997) The role of nonlinear combustion response in pulsed oscillations in rocket motors. *Combustion Science and Technology*, submitted.